Dynamics of Ion Beam Charge Neutralization by Ferroelectic Plasma Sources

Anton D. Stepanov, Erik P. Gilson, Larry R. Grisham, Igor D. Kaganovich, and Ronald C. Davidson

Princeton Plasma Physics Laboratory, Princeton University, P.O. Box 451, Princeton, New Jersey 08543

Abstract

Ferroelectric Plasma Sources (FEPSs) can generate plasma that provides effective space-charge neutralization of intense high-perveance ion beams, as has been demonstrated on the Neutralized Drift Compression Experiment NDCX-I and NDCX-II. This article presents experimental results on charge neutralization of a high-perveance 38 keV Ar^+ beam by a plasma produced in a FEPS discharge. By comparing the measured beam radius with the envelope model for space-charge expansion, it is shown that a charge neutralization fraction of 98% is attainable with sufficiently dense FEPS plasma. The transverse electrostatic potential of the ion beam is reduced from 15 V before neutralization to 0.3 V, implying that the energy of the neutralizing electrons is below 0.3 eV. Measurements of the time-evolution of beam radius show that near-complete charge neutralization is established $\sim$5 μs after the driving pulse is applied to the FEPS, and can last for 35 μs. It is argued that the duration of neutralization is much longer than a reasonable lifetime of the plasma produced in the sub-μs surface discharge. Measurements of current flow in the driving circuit of the FEPS show the existence of electron emission into vacuum which lasts for tens of μs after the high voltage pulse is applied. It is argued that the beam is neutralized by the plasma produced by this process, and not by a surface discharge plasma that is produced at the instant the high-voltage pulse is applied.

1. Introduction

Near-complete space-charge neutralization is required for the transverse compression of high-perveance ion beams for ion-beam-driven warm dense matter experiments and heavy ion fusion. One approach to beam neutralization is to fill the region immediately before the target with sufficiently dense plasma. The plasma provides a charge-neutralizing medium for beam propagation and makes it possible to achieve a high degree of compression beyond the space-charge limit. This approach was realized on the Neutralized Drift Compression Experiment-I (NDCX-I) [1, 2]. The large-volume plasma was produced by Ferroelectric Plasma Sources (FEPSs). Based on their performance on NDCX-I, FEPS plasma sources were selected for the upgraded experiment, NDCX-II [3], and are being considered for future heavy ion fusion drivers.

The operation of Ferroelectric Plasma Sources (FEPSs) is based on the surface discharge phenomenon in dielectrics with extremely high values of relative permittivity, such as barium titanate (ϵ_r ~1800) [4, 5, 6]. The basic configuration of a FEPS is a slab of ferroelectric material placed between two metal electrodes, one of which is segmented. Applying a fast-rising ($t_r < \mu$s) voltage pulse (~5 kV) to the solid electrode causes plasma formation around the segmented electrode at points of juncture between metal, ceramic, and vacuum, called triple points. The high value of ϵ_r is important for two reasons [7]: (a) amplification of the electric field at triple points in microgaps between metal and dielectric, and (b) the direction of the macroscopic electric field is primarily tangential to the surface of the dielectric. The primary electrons, produced by field emission in the microgaps, are accelerated by the tangential electric field along the surface of the dielectric, leading to the formation of an electron avalanche by secondary electron emission. A neutral layer forms by desorbtion and dielectric breakup [8]. The neutrals are ionized by the avalanche to form a plasma, which then expands outwards from the surface of the dielectric.

The plasma source used on NDCX (and in the present experiment) has a cylindrical cross-section (Fig. 1), with plasma production occurring at the inner surface covered by the segmented electrode. The ion beam propagates through the FEPS, where the plasma density can reach 5×10^{10} cm^{-3}, according to Langmuir probe measurements [9]. A plasma source based on a surface discharge has a number of advantages for charge neutralization of pulsed ion beams, such as easy integration into the beamline, and operation that does not interfere with the rest of the accelerator. In particular, neutral emission has to be minimal to maintain the high vacuum required for beam transport. Since the FEPS plasma is produced by ionization of solid dielectric material and neutral gas desorbed from the surface of the ceramic, no external gas feed is required. According to Ref. [10], near-complete charge neutralization can be obtained if the plasma density exceeds the ion beam density by a sufficiently large amount, and the plasma electron temperature is low compared to the magnitude of the space-charge potential of the beam.

Experimental results from NDCX-I confirm that the FEPS plasma satisfies these requirements.

The experiments on NDCX-I [1] were not focused on FEPS research. As a result, there is still a need for a comprehensive study of FEPS operation and performance optimization. In the present work, a 38 kV, perveance-dominated Ar^+ beam is used to study the effects of the FEPS plasma discharge on charge neutralization of the ion beam. The parameters of the Ar^+ beam are quite different compared to the NDCX beam, providing new insight about the parameters of the FEPS plasma. In particular, the space-charge potential of the 38 kV Ar^+ beam is about 15 V, compared to 150 V on NDCX-I, which means that electrons with much lower temperature ($T_e \ll 15$ eV) are required for effective neutralization. Unlike NDCX, which operated with short beam pulses, the beam pulse duration in the present experiment is much longer than the $\sim$50 μs FEPS plasma lifetime. Therefore, the complete time-evolution of the FEPS plasma can be inferred from the transverse profile measurements of the ion beam. Lastly, the low-velocity Ar^+ beam has a high cross section for charge-exchange, so the loss of ion beam current can be used as a diagnostic of the neutral density inside the FEPS.

The experiments described in this article demonstrate that near-complete charge neutralization (>98%) can be attained with FEPS plasma, corresponding to a reduction of the transverse space-charge potential of the beam from 15 V to 0.3 V, which is indicative of a low temperature ($T_e < 0.3$ eV) of the neutralizing electrons. Measurements of the time evolution of the transverse beam profile reveal that near-complete charge neutralization is established in about 5 μs after the high voltage pulse is applied to the FEPS.

The state of near-complete charge neutralization can last for as long as 35 μs. It is found that the duration of neutralization corresponds to the duration of ongoing current flow in the driving circuit of the FEPS. This suggests that plasma is produced continuously for tens of μs, contrary to the commonly accepted mechanism of plasma production in a sub-μs surface discharge.

The organization of this paper is as follows. The experiment is described in Section 2, including the parameters of the ion beam, the FEPS pulser circuit, and the data acquisition procedure. The experimental technique for obtaining an electron-free beam, which was necessary for the neutralization experiment, is described in detail. Section 3 contains a discussion of the results. The methods of data analysis for estimating the charge neutralization fraction and the neutral density inside the FEPS are described in Sections 3.1 and 3.2, respectively. Section 3.3 discusses the data on the time evolution of the beam radius in response to FEPS plasma formation. The results are compared to a model of the FEPS discharge which assumes that plasma production occurs in a sub-μs surface discharge. Conclusions are summarized in Section 4.

2. Experiment

In the present experiment, the argon beam is extracted from a multi-cusp RF plasma source with three-electrode (accel-decel) extraction optics and a 4 mm diameter extraction aperture. A 200 μs long beam pulse is produced every 3 seconds. The pressure in the propagation chamber was about 10^{-6} Torr due to the flow of neutral argon from the plasma ion source. The accelerator is operated at an extraction voltage $V_B = 38$ kV and beam current $I_B = 0.7$ mA, which was measured with a large Faraday cup that intercepted the whole beam 13 cm downstream of the extraction aperture. The corresponding dimensionless perveance $Q = I_B\sqrt{M}/[4\pi\epsilon_0\sqrt{2e}V_B^{3/2}]$ was 3.9×10^{-4}. The value of I_B (and hence Q) was set such that the initial divergence of the beam due to ion optics was minimized, i.e., the ion source was operated at "perveance match" conditions.

Figure 2 shows a schematic of the beamline used in the present experiments. The ion beam enters a FEPS located 13 cm downstream of the extraction aperture. The FEPS plasma source has a 7.6 cm inner diameter and is 12 cm long (Fig. 3). The FEPS, described in detail in Ref. [11], was developed for NDCX-II. Downstream of the FEPS, the beam is intercepted by a movable Faraday cup, collimated with a 0.1 mm by 50.8 mm slit, oriented horizontally. The collimated Faraday cup (CFC) is movable in the vertical direction. To measure the time-resolved current density profile of the beam $I(x,t)$, the CFC signal is recorded at 35 vertical (x) positions within ±2 cm of the beam centerline. The total beam current $I_B(t)$ at $z = 40$ cm can be calculated by integrating the current density profile $I(x,t)$:

$$I_B(t) = \int_{-2cm}^{+2cm} I(x,t)dx$$

For the ion beam in this experiment, the above calculation gives $I_B = 0.5$ mA, which differs from the value measured with the large Faraday cup (0.7 mA). By operating the ion source at different plasma densities, it was found that the values of I_B measured with the two diagnostics are linearly related. This justifies using the value of I_B obtained by integrating the CFC profiles as a relative measurement of I_B. The discrepancy cannot be wholly attributed to greater charge exchange losses at the location of the CFC, which are estimated to be 1.5% for the conditions of the experiment. A possible reason for the discrepancy is that the actual width of the CFC slit is narrower than 100 μm.

The FEPS is driven by a high voltage pulser (Fig. 1), which consists of a 141 nF storage capacitor and a thyratron switch. Initially, the capacitor is charged to a positive DC voltage. When the thyratron is triggered, the positive terminal of the capacitor is grounded, resulting in the application of a negative voltage pulse to the outer electrode of the FEPS. The FEPS was operated at two charging voltages of 5.5 kV and 6.5 kV.

2.1. Analysis of beam expansion

Our approach to studying neutralization dynamics is to infer the effective beam perveance from a measurement of the beam radius 40 cm downstream from the source. The expansion of the beam envelope $R(z)$ is described by the envelope equation:

$$\frac{d^2R}{dz^2} = \frac{f_e Q}{R} + \frac{\epsilon_\perp^2}{R^3} \tag{1}$$

where f_e is the fraction of unneutralized space charge and $\epsilon_\perp$ is the unnormalized transverse emittance. The transverse emittance was measured using the two-slit method to be about 2 mm·mrad. At $Q = 3.9\times10^{-4}$, the perveance term in Eq. (1) dominates the emittance term ($QR^2/\epsilon_\perp^2 \simeq 270$), so the emittance term can be ignored in our analysis. Thus, if the initial radius and divergence of the beam are known, the radius of the beam at the z-location of the diagnostic, which is measured experimentally, depends on the effective perveance Q_{eff} only.

In order to infer changes in Q_{eff} due to charge neutralization by electrons from the FEPS discharge, the beam has to be free of electrons from other sources. In practice, however, ion beams tend to self-neutralize, producing electrons by ionization of background neutrals and secondary electron emission. These electrons become trapped in the space-charge potential well of the ion beam, neutralizing its space charge. The accumulation of electrons was expected to proceed for tens of μs for the conditions of this experiment. Correspondingly, we expected to observe a decrease in beam radius in the course of the 200 μs-long beam pulse. However, measurements showed that the beam radius did not decrease with time, implying a lack of electron accumulation in our system. The measured dependence of beam radius on the perveance Q showed excellent agreement with the envelope equation (1) assuming a complete lack of neutralization ($f_e = 1$). It was concluded that the ion beam was fully space-charge dominated, with a neutralization fraction close to zero. Increasing the residual gas pressure to increase the rate of electron production did not improve neutralization. This suggested that the absence of space-charge neutralization was not due to insufficient electron production, but due to poor electron confinement in the potential well of the beam.

It was determined that electron loss occurred due to incomplete shielding of the plasma electrode of the ion source, which was biased to +38 kV. When a grounded conducting mesh was installed to isolate the plasma electrode from the propagation chamber (Fig. 2), neutralization of the ion beam by residual gas ionization was observed. Figure 4 plots measurements of the beam radius as a function of time at different residual gas pressures. It can be seen that the beam radius decreases with time, corresponding to the accumulation of electrons produced by residual gas ionization. As expected, the duration of electron accumulation decreased with increasing pressure from $\sim$200 μs at 1.7×10^{-6} Torr to $\sim$10 μs at 1.1×10^{-4} Torr. A reasonable explanation for the lack of electron accumulation before the shielding mesh was installed is the presence of fringe electric fields in the beam propagation region due to the high-voltage plasma electrode. The lack of electron confinement in the beam in the absence of the shielding mesh highlights the importance of the boundary conditions of the propagation region for low-energy ion beams. If a space-charge dominated beam is desired, the mechanism for electron loss can be deliberately introduced into the system.

The installation of the shielding mesh, which was necessary to keep the FEPS plasma out of the acceleration gap, resulted in the introduction of another source of neutralizing electrons. This presented a problem for measuring charge neutralization by FEPS plasma only. Fortunately, it was found that when a recently-triggered FEPS was placed in the beam path, the capture of electrons produced by gas ionization in the space-charge potential well of the beam ceased completely, even at increased neutral pressures. The presence of the FEPS had a similar effect on electron accumulation to the unshielded plasma electrode. This is evident from the fact that the transverse current density profiles matched the profiles measured in the absence of the shielding mesh. Furthermore, no decrease of the beam radius on the timescale of tens of μs was observed. Figure 5 plots the current in the collimated Faraday cup (CFC) at the beam centerline with and without the FEPS installed. Without the FEPS, the current in the central beamlet increases over time, corresponding to a decrease of the beam radius due to electron accumulation. On the other hand, the current in the central beamlet does not increase in time with the FEPS installed. The lack of electron accumulation can be attributed to the presence of a dielectric boundary in the beam propagation region, which can result in electron removal due to a secondary electron emission coefficient above unity [12]. However, this mechanism does not fully explain the observed effect because electron removal occurred only after the FEPS had been operated. This suggests that the FEPS dielectric retained a positive polarization surface charge after producing plasma, which decayed over several hours.

With electron removal by the FEPS, the beam had a charge neutralization fraction of approximately zero prior to triggering the FEPS, making it possible to attribute measured changes in the beam radius to the decrease in the effective perveance of the beam due to electrons produced in the FEPS plasma discharge.

2.2. Data Acquisition Procedure

The measurement of the ion beam current density profiles with the collimated Faraday cup (CFC) was complicated by the fact that charged particles emitted by the FEPS entered the CFC. To obtain accurate time-resolved current density measurements of the ion beam, the FEPS current was measured separately and subtracted from the ion beam current signal with FEPS neutralization. In order to prevent the bulk FEPS plasma electrons from entering the diagnostic, the suppressor and collector electrodes of the CFC were biased to -300 V and -400 V, respectively. The positive 100 V bias of the suppressor with respect to the collector was set so the SEE electrons generated at the collector are attracted to the suppressor grid, thus contributing to the current measured at the collector. This approach, used previously in

Ref. [13], effectively amplified the ion beam current signal by a factor of 8 without increasing the amplitude of the FEPS signal.

Typical unprocessed CFC signals, plotted in Fig. 6, show that the magnitude of the positive current due to the FEPS plasma ions is comparable to the ion beam signal. The FEPS signal shows significant shot-to-shot variation, so in order to subtract the FEPS contribution to the CFC signal, an average of six consecutive shots at each CFC position is used. The use of the background subtraction procedure is justified by calculating the total ion beam current as a function of time (Fig. 7). Besides the first 2 μs after the FEPS is triggered, the total ion beam current is approximately constant and equal to its initial value.

3. Results and Discussion

The time-evolution of the transverse size of the beam in response to the appearance of the FEPS plasma is plotted in Fig. 8. The transverse size of the beam is characterized by the RMS (X_{RMS}) and half-width, half-max (X_{HWHM}) widths of the profile. At V_{FEPS} = 5.5 kV, the minimum beam width was X_{HWHM} = 5.4 mm (X_{RMS} = 4.5 mm). The beam retained this minimal divergence for $\sim$7 μs. Afterwards, the beam divergence increased, but remained smaller than the unneutralized divergence for the recorded interval. Neutralization improved by increasing the FEPS driving voltage. At V_{FEPS} = 6.5 kV, the minimum transverse size of the beam was X_{HWHM} = 5.0 mm (X_{RMS} = 3.9 mm). The duration of neutralization increased significantly to $\sim$35 μs. For both charging voltages, the transition from the space-charge-dominated spot size to the fully-neutralized spot size occurred in about 5 μs after the FEPS is triggered.

3.1. Estimating the effective perveance with FEPS neutralization

Beam profiles before and after the FEPS is triggered, shown in Fig. 9, can be analyzed in terms of the envelope model [Eq. (1)] to estimate the effective beam perveance Q_{eff} attained with FEPS neutralization. Estimating Q_{eff} requires knowledge of 3 parameters: the initial beam radius (R_0), the initial divergence angle (R_0'), and the radius of the beam at the location of the diagnostic [$R(z = 40$ cm)]. It was found that the value of the initial radius R_0 does not strongly affect the estimate of Q_{eff}, so $R_0 = 1.5$ mm was assumed, which is equal to the radius of the extraction aperture of the ion source. The estimate of Q_{eff} is, however, very sensitive to the value of the initial divergence angle R_0', which cannot be measured directly. This is because it is impossible to achieve perfect charge neutralization, so some beam expansion will invariably occur due to nonzero effective perveance. It is possible to obtain an upper bound for R_0' from the envelope equation by assuming $Q_{eff} = 0$, but this approach is clearly not practical since the goal is to determine a non-zero value of Q_{eff}.

Unlike in the case of a neutralized beam, the perveance $Q \propto I_B/V_B^{3/2}$ of an unneutralized beam is known with good certainty based on the measured values of beam current I_B and accelerating potential V_B. With Q and R_0 known, the initial divergence angle R_0' can be inferred from the measured radius of the beam. This requires a systematic way of defining the beam radius from the transverse profile data. Note that for an axisymmetric beam, the transverse space charge force on a particle on the edge of the beam depends on the linear charge density $\lambda = I_B/v$, irrespective of the radial current density distribution. In theory, the radius of the outermost trajectory could be used to define the beam radius. However, the profiles measured experimentally typically show wide "tail" regions with no obvious edge of the beam, making it necessary to consider the whole profile in order to define the beam radius.

The shape of the profile must be consistent with expansion due to space charge. The simplest case to consider is that of a laminar beam with uniform radial current density $j(r)$:

$$j(r) = \begin{cases} I_B/(\pi R_B^2) & r \leq R_B \\ 0 & r > R_B \end{cases}, \quad R'(r) = R'_0 \cdot \frac{r}{R_B} \tag{2}$$

For a uniform profile, the radial electric E_r is proportional to radius, which means that the electric field due to space charge results in a linear defocusing force, i.e.,

$$E_r(r) = \frac{I_B r}{2\pi\epsilon_0 R_B^2 v} \ .$$

For a laminar beam subject to a linear force, the shape of the transverse profile must remain unchanged. Thus, the profile of an initially-uniform beam will remain uniform during space-charge expansion, with the radius $R_B(z)$ defined by the envelope equation (Eq.1). In the experiment, y-integrated current density profiles $I(x)$ were measured. For a beam with a uniform radial current density profile determined from Eq. (2), $I(x)$ is given by

$$I(x) = \int j(x,y)dy = \frac{2I_B}{\pi R_B}\sqrt{1 - x^2/R_B^2} \ . \tag{3}$$

The space-charge-dominated profile in Fig. 9 shows an excellent match with $I(x)$ defined by Eq. (3), with beam radius equal to 17.5 mm. The initial divergence angle can now be calculated from Eq. (1) to be 1.2°, assuming an initial beam radius of 1.5 mm and $Q = 3.9\times10^{-4}$. This result is in good agreement with previous studies of characteristic beam divergence of produced by plasma ion sources with 3-electrode extraction optics [14].

Assuming that the beam profile neutralized by the FEPS at 6.5 kV (Fig. 9) has a radius of 10 mm, which includes the whole peak of the profile, the effective perveance can be calculated from Eq. (1) to be $Q_{eff} = 0.02\ Q_0$. This degree of neutralization (98%) must exist along the whole length of the beam, which means that electrons produced in the FEPS discharge propagated throughout the volume of the beam. The radius of the profile obtained with gas neutralization is approximately equal to 11.3 mm, which corresponds to a charge neutralization fraction of 83%.

The estimated value of Q_{eff} with neutralization by FEPS plasma can be related to the amplitude of the transverse electrostatic potential $V_\perp$ of the beam, which is reduced from 15 V in the absence of neutralization to 0.3 V with $Q_{eff} = 0.02\ Q_0$. For neutralizing electrons to be trapped in the residual potential of the beam, their energy has to be below 0.3 eV, which provides an estimate of the temperature of the neutralizing electrons supplied by the FEPS. This is supported by the fact that neutralization by the FEPS plasma source driven at 6.5 kV results in a narrower beam profile than neutralization by gas ionization (Fig. 9). Note that the above electron temperature estimate does not apply to the bulk of the FEPS plasma, but only to the population of electrons produced in the FEPS discharge that neutralize the ion beam. A similar process of cold electron accumulation occurs in negative-glow plasmas [15].

Ref. [16] reports a charge neutralization fraction of 80% for a 0.4 mA, 160 keV Cs^+ beam neutralized by electrons emitted from a hot tungsten filament. Magnetic quadrupoles were used to give the beam a converging trajectory to the target, with the filament placed immediately downstream of the last focusing quadrupole. The main parameters that determine the degree of charge neutralization, which are the magnitude of the transverse electrostatic potential $V_\perp$ and the temperature of the neutralizing electrons T_e, are quite similar between Ref. [16] ($V_\perp = 7.5$ V, $T_e \sim 0.2$ eV) and the present experiment ($V_\perp = 15$ V, $T_e \sim 0.3$ eV). The greater degree of charge neutralization that was obtained in the present experiment can be attributed to the fact that electrons were extracted from a volume plasma, versus a localized emitter in Ref. [16]. This agrees with the results of Ref. [10], where different methods of charge neutralization are compared, and it is shown that introducing a volume plasma into the beam propagation region provides the greatest degree of charge neutralization.

3.2. Neutral density inside the FEPS

The loss of ion beam current to charge-exchange collisions can be used as a diagnostic of the neutral density inside the FEPS. Besides the small fluctuations of the current in the first 10 μs after the FEPS trigger, which are likely due to errors from background subtraction, no measurable decrease in ion beam current is detected for the first 40 μs (Fig. 7). By assuming that a small fraction of the ion beam current is lost, we can estimate an upper bound for the neutral density n_n inside the FEPS. For a neutral cloud with length $L = 12$ cm and a charge-exchange cross section $\sigma_{\mathrm{cx}} = 1.2\times10^{-15}$ cm^2, the loss fraction is

$$f_{loss} = 1 - \exp[-n_n \sigma_{\rm cx} L] \ . \tag{4}$$

For $f_{loss} = 1\%$, $n_n = 7{\times}10^{11}$ cm^{-3} ($n_n = 4{\times}10^{12}$ cm^{-3} for $f_{loss} = 5\%$). The value of σ_{cx} is based on measured beam current loss at $1.1{\times}10^{-4}$ Torr, and is in agreement with published cross-section data [17].

The data shows that the ion beam pulse is able to pass through the FEPS source well before the neutrals arrive. This is not a surprising result, given that the velocity of the neutral front is expected to be about 1 cm/ms [5]. For the short ion beam pulses envisioned for heavy ion fusion, the FEPS source can provide neutralizing plasma while keeping the beam propagation region neutral free.

3.3. Basic physics of FEPS operation

The traditional description of the FEPS plasma source operation [7] is based on the surface discharge phenomenon. The discharge is initiated by electron emission from metal-dielectric-vacuum triple points when the fast-rising voltage pulse is applied. These electrons are accelerated along the dielectric surface by a tangential electric field. An electron avalanche grows by secondary electron emission. Neutrals are desorbed from the surface and ionized by the avalanche, forming a thin layer of plasma near the surface of the dielectric. After formation, the plasma expands outwards, filling the volume of the FEPS. A key feature of this model is that all the plasma is formed in the sub-μs time interval required for the electron avalanche to traverse the surface of the dielectric. No other mechanisms of plasma formation are considered. The persistence of the plasma for tens of μs, which is observed experimentally, is sometimes described as "afterglow."

Based on the measured time evolution of the beam radius in response to FEPS plasma formation (Fig. 8), we can discuss the validity of the assumption that plasma formation occurs only in the first fraction of a μs. The first characteristic timescale of the FEPS is the delay between the application of the HV pulse and when the beam becomes fully neutralized, which is about 5 μs in our data. In the surface discharge model, this delay arises due to the propagation time of the plasma from the edge of the FEPS to the center. The characteristic velocity of propagation is the ion sound speed $v_s = (T_e/M_i)^{1/2}$. If $v_s = R_{FEPS}/5\mu s = 0.76$ cm/μs, then the electron temperature can be estimated ($T_e = v_s^2 M_i$) with an additional assumption for the ion mass M_i. If the FEPS plasma is composed of the $BaTiO_3$ ceramic, then using $M_i = 16$ amu (oxygen) gives $T_e = 10$ eV. Using M_i for titanium and barium gives unreasonably high T_e values. Another possibility is that the plasma is formed by ionization of the adsorbed neutral layer. For $M_i = 1$ amu (i.e. hydrogen from water vapor or pump oil), $T_e = 0.6$ eV.

A similar delay of 7 μs between triggering the FEPS and optimal beam neutralization was reported on NDCX-I [18]. This is somewhat surprising given the different parameters of the NDCX beam, which had a space-charge potential of 150 V, compared to 15 V for the Ar^+ beam in the present experiments. Since effective charge neutralization requires electrons with a much lower temperature than the space-charge potential energy of the ion beam, neutralization of the NDCX-I beam can be achieved by hotter (more mobile) electrons, which should reach the center of the FEPS sooner than the cold electrons required for neutralization in the present experiments. The fact that similar delays are observed can be attributed to electrostatic confinement of plasma electrons by the plasma ions. That is, free movement of plasma electrons inside the volume of the FEPS becomes possible only when the slow-moving plasma ions reach the center of the FEPS.

However, in the present experiment, the near-complete charge neutralization that was observed 5 μs after the FEPS trigger had to exist throughout the whole length of the beam. In particular, the beam had to be neutralized immediately downstream of the ion source, which was located 13 cm upstream of the FEPS. This experimental fact contradicts the notion that electron mobility is severely constrained by the ion space charge.

Another characteristic timescale of the FEPS plasma is the duration of neutralization. At $V_{FEPS} = 6.5$ kV, neutralization lasts for longer than 35 μs (Fig. 8). During the entire interval, the maximum neutralization fraction of 0.98 is maintained. Intuitively, one would expect that the plasma inside the FEPS should last approximately as long as the time it takes to propagate to the center, i.e. about 5 μs. According to a previous analysis of the dissipation of a high-density volume plasma produced by a laser pulse [19], the lifetime of the plasma is approximately equal to the time it takes to traverse the length of the system at the ion sound speed. This is confirmed by the direct measurement of the FEPS ion current in the CFC (Fig. 7). The data shows that the bulk of the ions emitted by the FEPS reach the diagnostic within 8 μs after the FEPS trigger. The FEPS ion current falls to the background level approximately 30 μs after the FEPS trigger. At this time, the ion beam is still fully neutralized.

A possible explanation for the 35 μs duration of neutralization is that the beam remains neutralized as long as the plasma density inside the FEPS exceeds a certain threshold density, e.g., the beam density ($n_b \sim 10^8$ cm^{-3}). The density of a dissipating plasma as a function of time can be modeled as an exponential decay with a characteristic time scale τ, which corresponds to the time it takes to traverse the radius of the FEPS at the ion sound speed, i.e.,

$$\frac{dn}{dt} = n_0 \mathrm{e}^{-\frac{t}{\tau}} = n_0 \mathrm{e}^{-\frac{v_s t}{R}} \ . \tag{5}$$

Here n_0 is the initial plasma density, R is the radius of the FEPS, and $v_s = (kT_e/M_i)^{1/2}$ is the ion sound speed. For $\tau = 5$ μs, the initial plasma density inside the FEPS can be estimated to be $n_0 \sim 1.1{\times}10^{11}$ cm^{-3}, assuming that at $t = 35$ μs the plasma density becomes equal to the beam density ($n_b = 10^8$ cm^{-3}). This estimate exceeds previous measurements of the density in the center of the FEPS [11] by a factor of $\sim$2.

The inconsistency between experimental data and the model of plasma production in a sub-μs surface discharge has been encountered in previous work on ferroelectric cathodes [20], where plasmas lasting longer than 30 μs after the driving pulse has been removed were observed. The authors describe this as an "anomalous" result. Overall, the surface discharge model of FEPS operation is contradicted by the experimental data in several important ways. An alternative explanation for the observed temporal dynamics of neutralization is continuous emission of electrons by the FEPS, which lasts for tens of μs after the high-voltage pulse. It is likely that the nature of this emission involves ferroelectric properties of barium titanate. Possibly, the application of the high voltage pulse establishes a highly non-equilibrium polarization state. The subsequent electron emission serves as a relaxation mechanism.

Preliminary evidence of this emission was obtained in a separate set of experiments, in which the forward current I_{frw} to the outer electrode of the FEPS and the return current I_{ret} from the segmented electrode to ground were measured (Fig. 1). It was found that a forward current of several amperes continues to flow to the outer electrode for tens of μs after the high-voltage pulse is applied. This current was conducted through the thyratron, which remained in the afterglow state. This demonstrates the presence of ongoing energy exchange and charge exchange between the FEPS and the external circuit well after the HV pulse, which could drive continuous charged-particle emission. We also observed a significant difference of several amperes between the return and forward currents, corresponding to emission of negative charge into vacuum, which was confirmed with Faraday cup measurements. The emission current was found to last for tens of μs after the application of the high voltage pulse. Figure 10 shows plots of the waveforms of the current emitted by the FEPS for charging voltages of 6.5 and 5.5 kV, together with the electron current measured in the Faraday cup. The data shows very good correspondence between the current "missing" in the circuit and the charged particle current in the Faraday cup.

The fact that plasma formation can occur well after the application of the high-voltage pulse is also evident from fast photography studies of the FEPS discharge (Fig. 11), which were carried out for the compact (3.5 cm diameter) FEPS in Ref. [18]. Figure 11 shows that the formation and dissipation of the surface discharge plasma occurs in the first $\sim$4 μs after the FEPS is triggered, with a secondary discharge appearing $\sim$6 μs after the FEPS is triggered. The timing of the secondary discharge agrees with the 5 μs delay between the application of the driving pulse to the FEPS and near-complete charge neutralization of the ion beam in the present experiments. While further investigation is required to establish the detailed nature of this emission, we believe it is the likely mechanism responsible for producing the electrons that neutralize the ion beam space charge in the operation of ferroelectric plasma sources.

4. Conclusions

The experimental results confirm that FEPS plasma sources are effective for charge neutralization of high-perveance ion beams. At a 6.5 kV FEPS charging voltage, the degree of charge neutralization by FEPS plasma was estimated to be up to 98%, implying very low temperature of the neutralizing electrons. It was also determined that the central region was free of neutrals during the first 40 μs after the initiation of the FEPS plasma discharge.

Based on the measured time-evolution of the beam radius in response to the formation of the FEPS plasma, the nature of the basic mechanism by which the plasma is formed was addressed. The data shows that optimal neutralization is established by 5 μs after the high-voltage pulse, and can last for longer than 35 μs. In the widely accepted model of plasma formation, which is based on the propagation of an electron avalanche along the surface of the dielectric, plasma production occurs only in a fraction of a μs when the high-voltage pulse is applied. It is suggested that the measured 35 μs duration of neutralization is significantly longer than the predicted lifetime of such plasma, which is estimated from the size of the system and the ion sound speed. In addition, it was determined that the electrons produced in the FEPS discharge filled the whole length of the ion beam by 5 μs after the FEPS was triggered. This result directly contradicts the notion that the mobility of the FEPS plasma electrons is restricted by the space-charge of the slow-moving FEPS plasma ions, which is required to explain the 5 μs neutralization delay according to the surface discharge model.

An alternative explanation of the experimental data is that charge is emitted by the FEPS continuously for tens of μs after the application of the high-voltage pulse. Then, the timing of the ion beam neutralization can be naturally attributed to the inherent duration of this emission process, without having to justify the presence or absence of plasma to explain specific experimental measurements. Preliminary experimental results were presented in support of the continuous emission hypothesis. Our measurements show that after the high-voltage pulse is applied, several amperes of current continue to flow in the pulser circuit to the outer electrode of the FEPS for tens of μs. This current is likely to provide energy and charge for charged particle emission by the FEPS. In addition, we measured the emission of negative charge by the FEPS into vacuum with a Faraday cup.

Although our measurements indicate that electron emission into vacuum indeed exists, the exact physical nature of this process remains unclear and merits further research. It is likely that this emission process, and not surface discharge plasma, is essential to the operation of ferroelectric plasma sources. It is worth noting that we do not dispute the fact that plasma formation by surface discharge occurs in the FEPS discharge. The essential aspect of our claim is that there exists another mechanism by which charged particles are emitted into vacuum continuously in the course of the FEPS discharge. The electrons produced by this mechanism are the ones responsible for the charge neutralization of high-perveance ion beams.

5. Acknowledgments

This research was supported by the U.S. Department of Energy contract DE-AC0209CH11466.

Figures

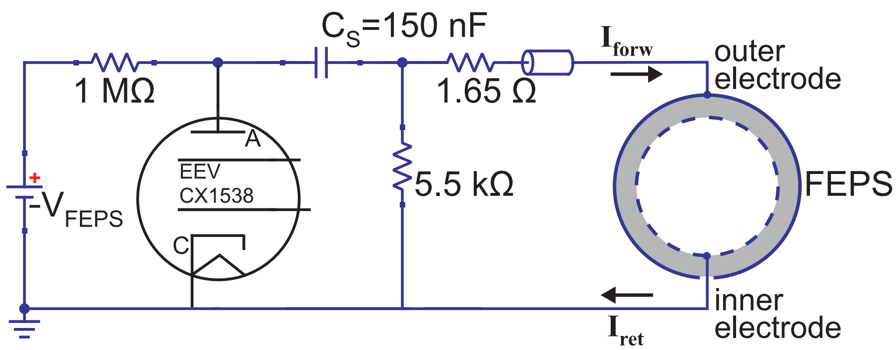

Figure 1: Schematic of the FEPS and the high-voltage pulser circuit. Initially, the 150 nF capacitor C_S is charged at a positive voltage V_{FEPS}. When the thyratron is triggered, the positive terminal of the capacitor is shorted to ground, and a negative voltage pulse is applied to the outer electrode of the FEPS. A difference in the forward electron current (I_{forw}) to the FEPS and the return current (I_{ret}) to ground is indicative of charged particle emission by the FEPS.

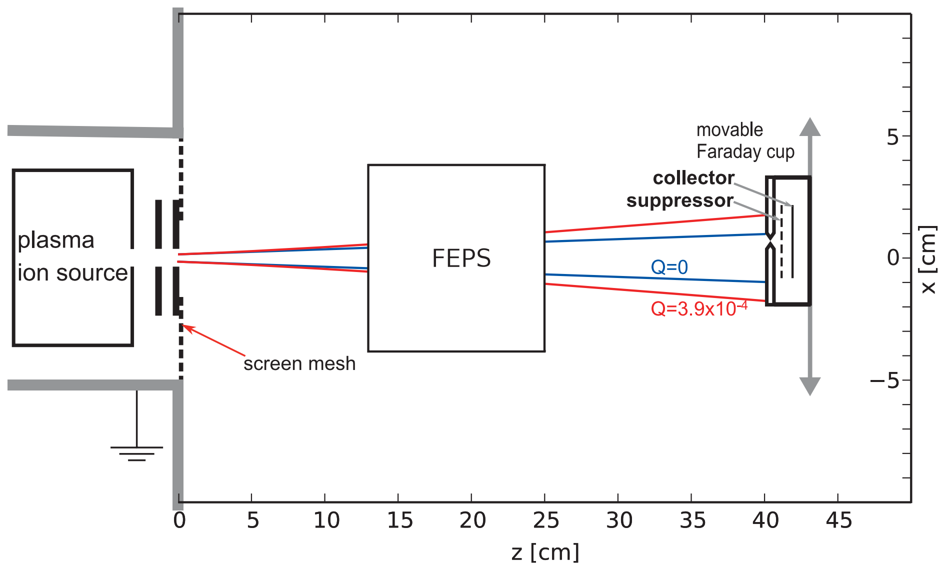

Figure 2: Experimental beamline arrangement. An Ar^+ beam, extracted from a plasma ion source, propagates through a cylindrical FEPS. Solutions to the envelope equation Eq. (1) are plotted for $Q = 3.9{\times}10^{-4}$ (red) and and $Q = 0$ (blue), with $R_0 = 2$ mm and $R_0' = 1.2°$ assumed for both envelopes. Downstream of the FEPS, the beam is intercepted by a movable collimated Faraday cup at $z = 40$ cm, which is used to measure the transverse current density profile of the beam.

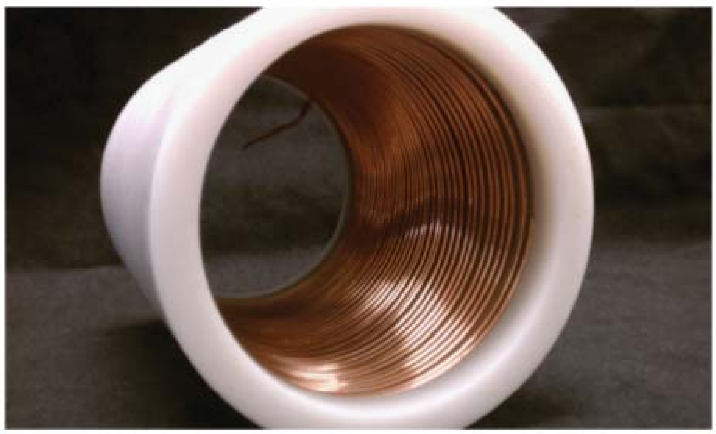

Figure 3: Ferroelectric plasma source (FEPS) that was used in the experiment. The grounded inner electrode is a helical stainless steel winding with a 2 mm pitch. The diameter of the winding is slightly larger than the inner diameter of the $BaTiO_3$ cylinder, ensuring good contact between the inner electrode and the ceramic. The ceramic cylinder is enclosed in a Delrin jacket to prevent electrical breakdown.

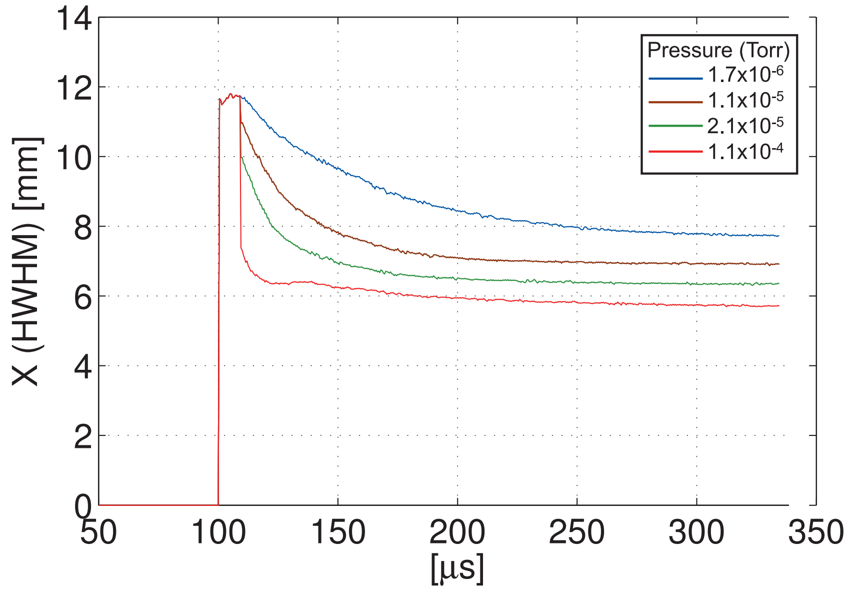

Figure 4: Time-evolution of transverse beam size ($X_{HWHM}(t)$) at different chamber pressures. The accelerating voltage is applied at $t = 100$ μs and turned off at $t = 380$ μs. It can be seen that the transverse beam size decreases faster as the pressure is increased due to an increase in the rate of electron production by the ion beam.

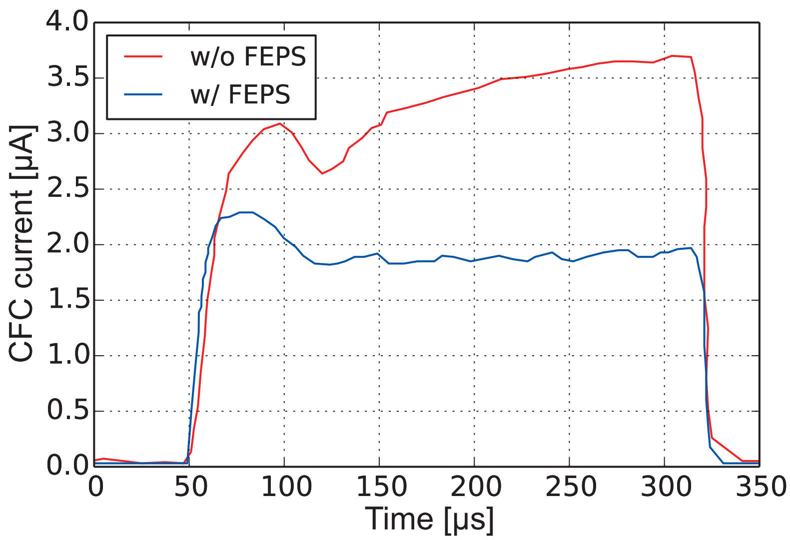

Figure 5: Plot of current density on the beam axis versus time with electron removal by a FEPS (blue trace) and with autoneutralization (red trace). The accelerating voltage is applied at $t = 50$ μs and turned off at $t = 330$ μs. The increase in current on the beam axis is observed when electrons are not prevented from accumulating in the beam potential well (red trace). On the other hand, the current on the beam axis does not increase in time with the FEPS in the beamline (blue trace), which implies a lack of electron accumulation in the beam.

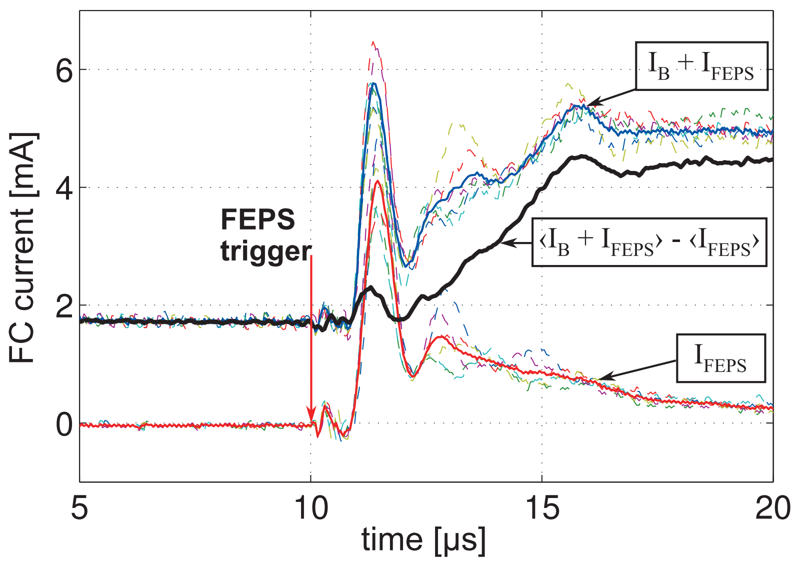

Figure 6: Typical collimated Faraday cup current signals: (blue) average of combined ion beam and FEPS currents ($\langle I_B + I_{FEPS}\rangle$); (red) average FEPS-only current ($\langle I_{FEPS}\rangle$); and (black) ion beam current with the FEPS background subtracted ($\langle I_B + I_{FEPS}\rangle - \langle I_{FEPS}\rangle$). Averages of six signals were used because the FEPS current varied somewhat between individual shots (dashed lines).

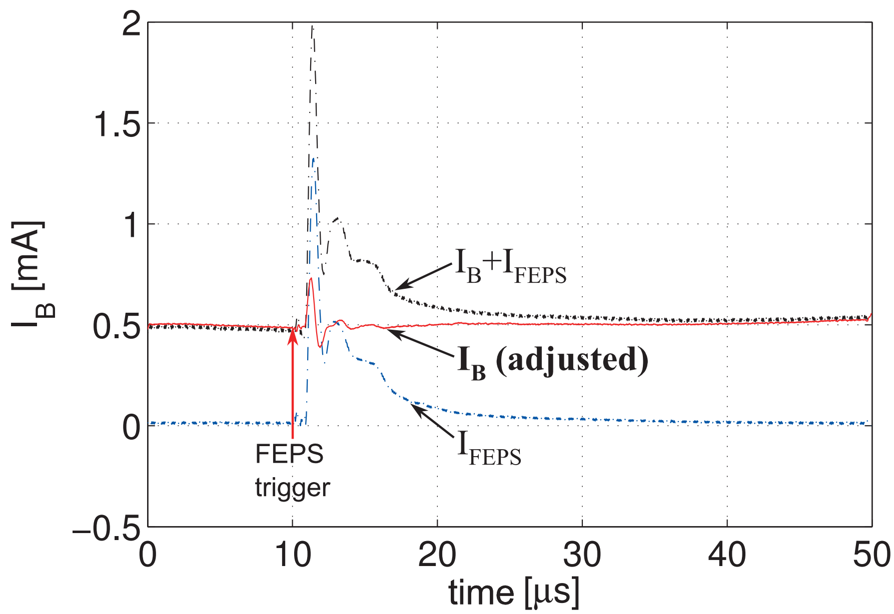

Figure 7: Total current as a function of time calculated by integrating the current density profiles. The total beam current I_B adjusted for the FEPS background stays approximately constant after the FEPS is triggered, confirming the accuracy of the FEPS background subtraction.

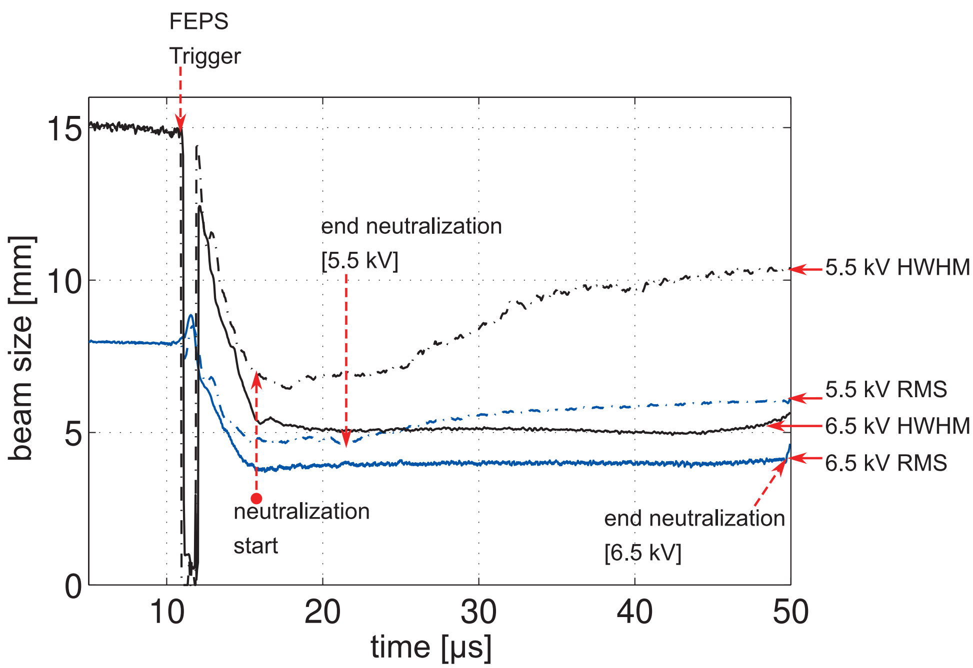

Figure 8: The time evolution of the transverse size of the beam in response to FEPS plasma formation. Full neutralization is established about 5 μs after the FEPS is triggered. For V_{FEPS}=6.5 kV, full neutralization lasts for about 35 μs.

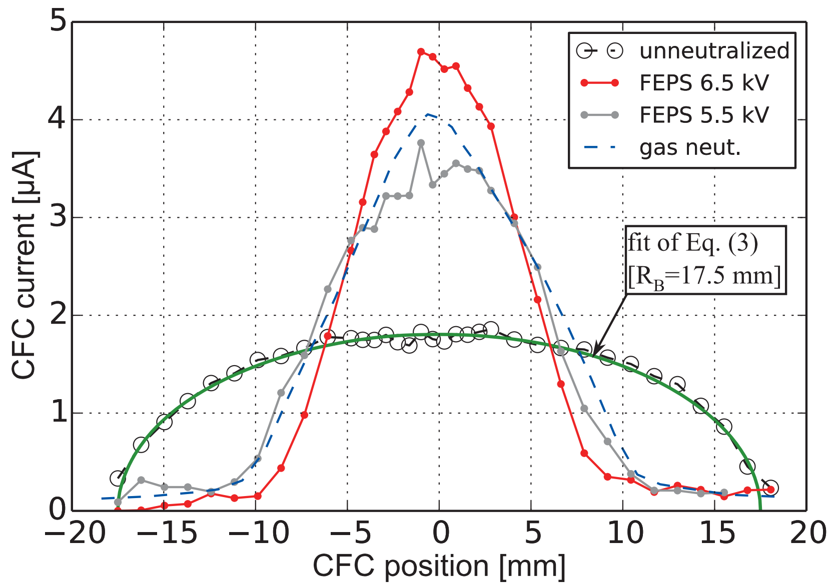

Figure 9: Transverse density profiles of the space-charge-dominated and neutralized beam. The shape of the space-charge-dominated profile, obtained at $t = 10.0$ μs, corresponds a beam with radius 17.5 mm and uniform current density given by Eq. (3) (green curve). The profiles neutralized by the FEPS are shown at $t = 20.5$ μs for $V_{FEPS} = 6.5$ kV, and at $t = 18.0$ μs for $V_{FEPS} = 5.5$ kV. The plot of the least divergent profile obtained with neutralization by gas ionization (pressure $= 2\times10^{-5}$ Torr of air) is included to demonstrate that FEPS neutralization can produce a less divergent beam than neutralization by gas ionization, which is indicative of lower electron temperature in the FEPS plasma.

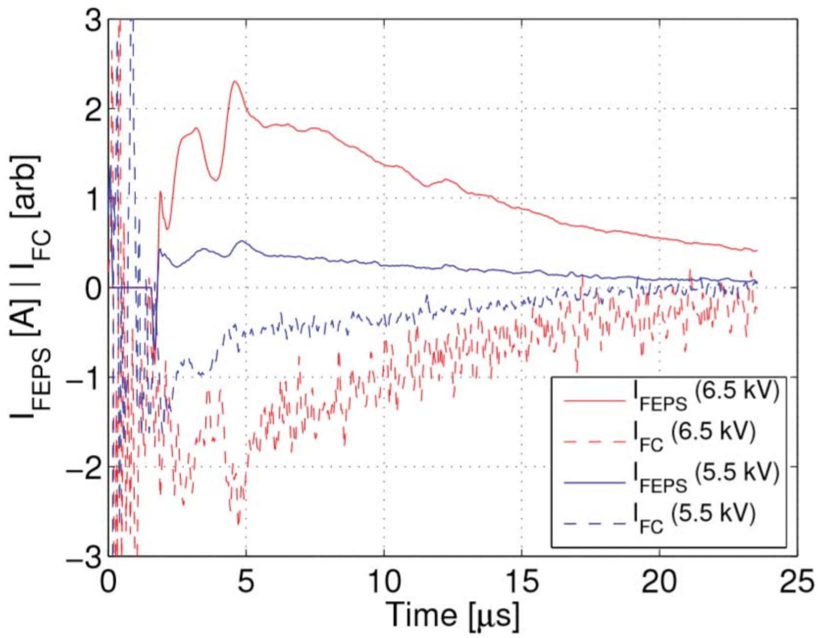

Figure 10: Waveforms of electron current emission by the FEPS source ($I_{FEPS} = I_{frw} - I_{ret}$) for charging voltages of 6.5 kV and 5.5 kV. The dashed lines are the currents to the Faraday cup (I_{FC}). The fact that the "missing" current in the circuit (I_{FEPS}) corresponds to the electron emission is evident from the similar time evolution of I_{FEPS} and I_{FC}.

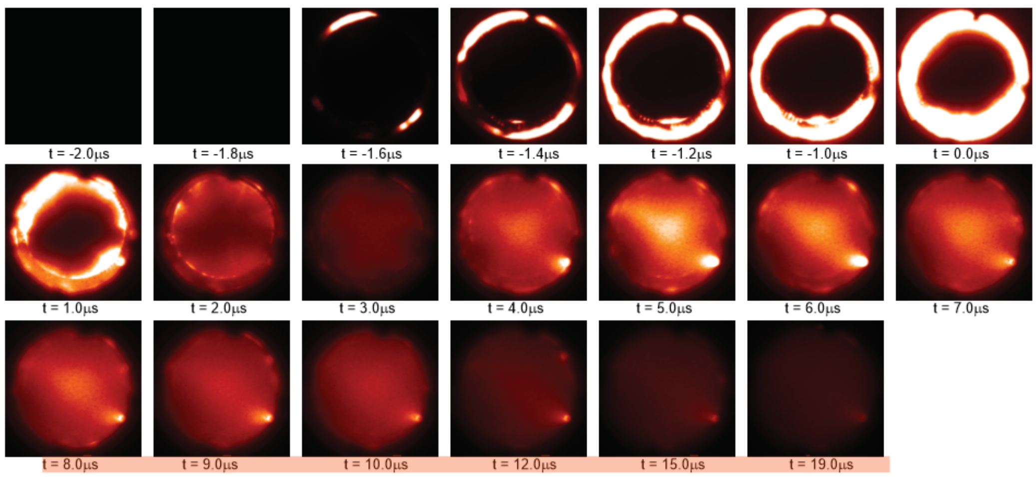

Figure 11: Fast photography images of the compact FEPS in Ref. [18]. The images are averages of 8 consecutive FEPS shots taken with a 1 μs exposure. The FEPS is triggered at $t = -1.8$ μs. After the formation and dissipation of the surface discharge plasma by $t = 2.0$ μs, a secondary discharge is initiated at $t = 4.0$ μs. The initiation of the secondary discharge occurs approximately when the beam attains near-complete charge neutralization in the present experiment. This suggests that the plasma produced in the secondary discharge is responsible for the near-complete charge neutralization of the ion beam.

References

[1] P.K. Roy, S.S. Yu, E. Henestroza, A. Anders, F.M. Bieniosek, J. Coleman, S. Eylon, W.G. Greenway, M. Leitner, B.G. Logan, W.L. Waldron, D.R. Welch, C. Thoma, E.P. Gilson, P.C. Efthimion, and R.C. Davidson. Phys. Rev. Lett. **95**, 234801 (2005).

[2] P.A. Seidl, A. Anders, F.M. Bieniosek, J.J. Barnard, J. Calanog, A.X. Chen, R.H. Cohen, J.E. Coleman, M. Dorf, and E.P. Gilson. Nucl. Instrum. Methods Phys. Res. A **606**, 75 (2009).

[3] W.L. Waldron, W.J. Abraham, D. Arbelaez, A. Friedman, J.E. Galvin, E.P. Gilson, W.G. Greenway, D.P. Grote, J-Y Jung, J.W. Kwan, M. Leitner, S.M. Lidia, T.M. Lipton, L.L. Reginato, M.J. Regis, P.K. Roy, W.M. Sharp, M.W. Stettler, J.H. Takakuwa, J. Volmering, and V.K. Vytla. Nucl. Instrum. Methods Phys. Res. A **733**, 226 (2014).

[4] G. Rosenman, D. Shur, Ya.E. Krasik, and A. Dunaevsky. J. Appl. Phys. **88**, 6109 (2000).

[5] Y.E. Krasik, K. Chirko, A. Dunaevsky, J.Z. Gleizer, A. Krokhmal, A. Sayapin, and J. Felsteiner. IEEE Trans. Plasma Sci. **31**, 49 (2003).

[6] V.Tz. Gurovich, Y.E. Krasik, V. Raichlin, J. Felsteiner, and I. Haber. J. Appl. Phys. **106**, 053301 (2009).

[7] G.A. Mesyats. Physics-Uspekhi **51**, 79 (2008).

[8] D. Yarmolich, V. Vekselman, V. Tz. Gurovich, and Ya. E. Krasik. Phys. Rev. Lett. **100**, 075004 (2008).

[9] P.C. Efthimion, E.P. Gilson, L. Grisham, R.C. Davidson, B.G. Logan, P.A. Seidl, and W. Waldron. Nucl. Instrum. Methods Phys. Res. A **606**, 124 (2009).

[10] I.D. Kaganovich, R.C. Davidson, M.A. Dorf, E.A. Startsev, A.B Sefkow, A.F. Friedman and E.P. Lee, Phys. Plasmas **17**, 056703 (2010).

[11] E.P. Gilson, R.C. Davidson, P.C. Efthimion, I.D. Kaganovich, J.W. Kwan, S.M. Lidia, P.A. Ni, P.K. Roy, P.A. Seidl, W.L. Waldron, J.J. Barnard, and A. Friedman. Nucl. Instrum. Methods Phys. Res. A **733**, 75 (2014).

[12] S.V. Dudin, A.V. Zykov, and V.I. Farenik. Rev. Sci. Instrum. **65**, 1451 (1994).

[13] S.A. MacLaren. University of California, Berkeley, PhD thesis, (2000).

[14] L.R. Grisham, C.C. Trai, J.H. Whealton, and W.L. Stirling. Rev. Sci. Instrum. **48**, 1037 (1977).

[15] Y.P. Raiser. *Gas Discharge Physics.* Springer, New York (1991); R.R. Arslanbekov and A.A. Kudryavtsev. Phys. Rev. E **58**, 6539, (1998).

[16] S.A. MacLaren, A. Faltens, P.A. Seidl, and D.V. Rose, Phys. Plasmas **9**, 1712 (2002).

[17] I. S. Griogoryev and E. Z. Meilikhov, editors. *Physical quantities: Reference book.* Moscow Energoatomizdat (1990).

[18] E.P. Gilson, R.C. Davidson, P.C. Efthimion, J.Z. Gleizer, I.D. Kaganovich, and Y.E. Krasik. Laser Part. Beams **30**, 435 (2012).

[19] K. Patel and V.K. Mago. J. Appl. Phys. **78**, 4371 (1995).

[20] K. Chirko, V.Ts. Gurovich, Ya. E. Krasik, O. Peleg, and J. Felsteiner. Phys. Plasmas **11**, 3865 (2004).